Nanoscale

PAPER

View Article Online
View Journal

Cite this: DOI: 10.1039/c5nr07257c

Shape controllers enhance the efficiency of graphene–TiO_2 hybrids in pollutant abatement†

F. Sordello,[a,b] E. Odorici,[a] K. Hu,[b] C. Minero,[a] M. Cerruti[b] and P. Calza*[a]

Received 19th October 2015,
Accepted 7th January 2016

DOI: 10.1039/c5nr07257c

www.rsc.org/nanoscale

The addition of graphene nanoplatelets (GNP) to TiO_2 nanoparticles (NPs) has been recently considered as a method to improve the photocatalytic efficiency of TiO_2 by favoring charge carrier separation. Here, we show that it is possible to improve the efficiency of GNP–TiO_2 composites by controlling the shape, stability, and facets of TiO_2 NPs grown on GNP functionalized with either COOH or NH_2 groups, while adding ethylendiamine (EDA) and oleic acid (OA) during a hydrothermal synthesis. We studied the photocatalytic activity of all synthesized materials under UV-A light using phenol as a target molecule. GNP–TiO_2 composites synthesized on COOH-functionalized GNP, exposing {101} facets, were more efficient at abating phenol than those synthesized on NH_2-functionalized GNP, exposing {101} and {100} facets. However, neither of these composites was stable under irradiation. The addition of both OA and EDA stabilized the materials under irradiation; however, only the composite prepared on COOH-functionalized GNP in the presence of EDA showed a significant increase in phenol degradation rate, leading to results that were better than those obtained with TiO_2 alone. This result can be attributed to Ti–OH complexation by EDA, which protects GNP from oxidation. The orientation of the most reducing {101} facets toward GNP and the most oxidizing {100} facets toward the solution induces faster phenol degradation owing to a better separation of the charge carriers.

1. Introduction

Many pollutants can be abated by photocatalysis, yielding carbon dioxide and dilute acids as final products.[1–6] TiO_2 nanoparticles (NPs) are one of the most widely used photocatalysts,[7] although their efficiency is limited by the fast recombination of the generated electron–hole pairs.[8,9] Many researchers have tried to improve TiO_2 photocatalytic activity[10–12] with strategies including surface modification with metal particles,[13,14] semiconductor coupling,[15,16] or the use of carbon nanotubes (CNTs) as support.[17,18] More recently, graphene was suggested as a material able to enhance TiO_2 photocatalytic efficiency by hindering the charge recombination process[19–22] thanks to its high charge carrier mobility.[23,24]

The phase, size, shape and extent to which different TiO_2 facets are developed govern TiO_2 activity.[25,26] While the {101} facets are the most thermodynamically stable in TiO_2 anatase, the {001} facets exhibit higher reactivity[27] and enhanced oxidising ability[28] (Scheme S1 in ESI†). Indeed, Ohno and coworkers[29] demonstrated that photogenerated holes and electrons can be trapped onto different TiO_2 surfaces, namely electrons on {101} and holes on {001} facets, leading to charge carrier separation.

On properly designed TiO_2 NPs, with both kinds of facets sufficiently developed, charge carrier recombination could be further suppressed thanks to coupling to graphene, which can scavenge electrons from TiO_2.[30] This synergistic effect can rise, provided that the most reducing {101} facets are exposed towards graphene, while the most oxidising {001} facets are in contact with the solution, thus maximising the degradation of dissolved organic compounds.

In a previous work, we used functionalized graphene nanoplatelets (GNP) as a substrate to control the phase, shape and exposed facets of TiO_2 NPs in GNP–TiO_2 nanocomposites.[31] We showed that both amino and carboxylate functions on GNP (designed as NH_2–GNP and COOH–GNP, respectively) were able to change the morphology of TiO_2 NPs grown during hydrothermal synthesis, and we reported for the first time TiO_2 NPs resting on graphene sheets with the most reducing {101} facets.

In the present work, we measure the photocatalytic activity towards the degradation of phenol of NH_2–GNP–TiO_2 and COOH–GNP–TiO_2, and we extend the range of GNP–TiO_2 composites by adding shape controllers during the hydrothermal synthesis to improve their catalytic activity and stability under

[a]Department of Chemistry, University of Turin, Via Giuria, 5, I-10125 Turin, Italy. E-mail: paola.calza@unito.it; Fax: +390116705242; Tel: +390116705268
[b]Materials Engineering, McGill University, 3610 University St., Montreal, QC H3A 0C5, Canada

†Electronic supplementary information (ESI) available. See DOI: 10.1039/c5nr07257c

irradiation. We selected either ethylendiamine (EDA) or oleic acid (OA) because they are known to favor the growth of different crystalline facets, namely {100} and {101} for EDA and {001} for OA, leading to elongated or pseudo-cubic anatase particles, respectively.[32] Owing to EDA or OA complexation, these facets will not be in close proximity to GNP, but they will likely be oriented towards the solution, thus affecting the charge carrier separation process and therefore the photoactivity and stability of the hybrid materials.

In principle, shape controllers may compete with GNP surface functions (COOH or NH_2) for TiO_2 surface sites; however, we observed[31] that the complexing ability of GNP surface groups is limited, and their effect on TiO_2 NP shape is due to local pH changes during NP growth. Still, the addition of shape controllers, in the absence of GNP complexation, may deeply affect the interaction between functionalized GNP and TiO_2. Indeed, our results demonstrate that the addition of EDA or OA leads to the formation of composites with different degrees of association between GNP and TiO_2 NPs. We find that loose coupling can be beneficial for both material stability and photocatalytic activity, and that composites formed on COOH–GNP in the presence of EDA as shape controller provide larger and stable photocatalytic activity than TiO_2 alone.

2. Experimental

2.1. Materials

Graphene nanoplatelets (GNP) were purchased from Graphene Supermarket (3 nm flakes, grade AO1, specific surface area 510 $m^2\ g^{-1}$). 4-aminophenyl acetic acid (ACS reagent 99%), sodium nitrite, hydrochloric acid 0.5 M, thionyl chloride ($SOCl_2$), ethylenediamine (EDA, ACS reagent 99%), isopropyl alcohol, titanium(IV) isopropoxide (TIP, ACS reagent 97%), triethanolamine (TEOA, ACS reagent 99%), oleic acid (OA, ACS reagent 99%) and phenol were all purchased from Aldrich and used as received without further purification. Acetonitrile (AC0331 Supergradient HPLC grade eluent) was purchased from Scharlau. All aqueous solutions were prepared with ultrapure Millipore Milli-Q™ water.

2.2. Synthesis of TiO_2–GNP composites

GNP with either carboxylic (COOH–GNP) or amino (NH_2–GNP) groups were prepared and coupled to TiO_2 by synthesizing TiO_2 NPs *in situ*, directly on the functionalized GNP either with or without the addition of OA or EDA as shape controllers.

2.2.1 Graphene surface modification

2.2.1.1 Carboxylic groups. COOH–GNP samples were prepared using diazonium chemistry as described in ref. 31 and Scheme S2.† Details on the synthetic procedure are reported in ESI.†

2.2.1.2 Amino groups. We synthesized NH_2–GNP samples *via* chlorination and amidation of COOH–GNP as described in ref. 31 and Scheme S2.† Details on the synthetic procedure are reported in ESI† and ref. 33.

Table 1 Samples studied in the present work

Name	Functional group on GNP	TiO_2	Shape controller
GNP	None	None	None
NH_2–GNP	NH_2	None	None
COOH–GNP	COOH	None	None
TiO_2	NO GNP	Yes	None
TiO_2–EDA	NO GNP	Yes	EDA
TiO_2–OA	NO GNP	Yes	OA
NH_2–GNP–TiO_2	NH_2	Yes	None
NH_2–GNP–TiO_2–EDA	NH_2	Yes	EDA
NH_2–GNP–TiO_2–OA	NH_2	Yes	OA
COOH–GNP–TiO_2	COOH	Yes	None
COOH–GNP–TiO_2–EDA	COOH	Yes	EDA
COOH–GNP–TiO_2–OA	COOH	Yes	OA

2.2.2 Graphene–TiO_2 coupling. We prepared GNP–TiO_2 samples by synthesizing TiO_2 NPs directly on GNP with a hydrothermal method.[31] Similarly to ref. 31, we used the Ti–TEOA 1 : 2 complex as precursor for TiO_2, prepared by pouring 50.0 mmol of titanium(IV) isopropoxide (TIP) in 100 mmol of triethanolamine (TEOA) and bringing to 100.0 mL with deionized water. We put 6.00 mL of the TIP–TEOA precursor in a Teflon-lined autoclave together with 7.5 mg of functionalized GNP, to have 3% GNP nominal content in all materials, and, in some of the samples, also 0.06 mmol of shape controller, either OA or EDA. We brought the volume of the mixture to 60 mL and adjusted the pH to a value between 9.5 and 10. The hydrothermal treatment took place at 110 °C for 24 h and then at 145 °C for 72 h.

To compare the photocatalytic activity of the hybrid materials with that of TiO_2 alone, we prepared TiO_2 NPs under the same conditions, with or without addition of EDA and OA, and carried out their hydrothermal synthesis in the absence of GNP.

Table 1 summarizes all the samples studied in this work.

2.3. Photocatalytic tests

We chose phenol as a target molecule to investigate the photocatalytic efficiency of the materials synthesized in this work. We placed 5 mL of an aqueous solution containing phenol (10 mg L^{-1}) and the catalyst at the desired concentration in Pyrex glass cells and irradiated the solution under stirring, using a TL K05 UV/A lamp with 25 mW m^{-2} power and emission maximum at 365 nm. We ran all the experiments using a catalyst suspension at a concentration of 1 g L^{-1} when using TiO_2-based materials. The suspension pH values were as follows: COOH–GNP–TiO_2 pH = 5.45, COOH–GNP–TiO_2–EDA pH = 5.62, COOH–GNP–TiO_2–OA pH = 4.96, NH_2–GNP–TiO_2 pH = 5.50, NH_2–GNP–TiO_2–EDA pH = 5.52, NH_2–GNP–TiO_2–OA pH = 5.10. We ran all the experiments by preparing a suspension with concentration of 25 mg L^{-1} when using GNP or functionalized GNP. After illumination, the entire content of each

cell was filtered through a 0.45 μm filter in order to eliminate the catalyst and then analyzed *via* HPLC/UV.

We followed the disappearance of phenol as a function of irradiation time using high-pressure liquid chromatography (HPLC, Merck-Hitachi L-6200 pumps) equipped with a Rheodyne injector, an RP C18 column (Lichrochart, Merck, 12.5 cm × 0.4 cm, 5 μm packing) and a UV-vis detector (Merck Hitachi L-4200) set at 220 nm. We eluted the samples with acetonitrile and phosphate buffer (0.01 M) at pH 2.8 (40 : 60% v/v) at a flow rate of 1 mL min^{-1}.

3. Results and discussion

3.1. Photo-induced phenol degradation with functionalized GNP/TiO_2 hybrids

By functionalizing GNP with either carboxylic (COOH) or primary amino (NH_2) groups, we were able to control the phase, shape and exposed facets of TiO_2 nanoparticles in GNP–TiO_2 nanocomposites, as shown in ref. 31. NH_2 groups favored the growth of TiO_2 bipyramids with higher truncation ratio than those synthesized on GNP modified with COOH groups (Fig. S1†). Also, NH_2 functionalization favored the coupling between GNP and {001} or {100} anatase facets, whereas COOH groups favored the coupling between GNP and {101} facets. This implies that the TiO_2 NPs found in COOH–GNP–TiO_2 exposed mostly the {001} facets towards the environment. Owing to the different properties of anatase {001} and {101} facets, the materials synthesized are likely to behave differently under irradiation and, consequently, have different photocatalytic activity. Specifically, since the {001} facets in TiO_2 are known to be more oxidizing, we expected the COOH–GNP–TiO_2 composite material to be more efficient at phenol abatement than the NH_2–GNP–TiO_2 material.

We tested phenol abatement on all materials reported in Table 1. Preliminary experiments on pristine GNP, COOH–GNP and NH_2–GNP allowed us to determine the best experimental conditions: due to their dark color, we resorted to using only a very low concentration of these materials (25–50 mg L^{-1}), whereas we could increase the catalyst concentration up to 1 g L^{-1} for the hybrid materials also containing TiO_2.

Adsorption experiments in the dark showed that phenol was poorly adsorbed on all materials (Fig. S2†). Direct photolysis scarcely contributed to phenol transformation, too: its degradation was negligible even after long irradiation times, as previously reported.[34]

Phenol disappearance curves are plotted in Fig. 1A. GNP and functionalized GNP (COOH–GNP and NH_2–GNP) were not able to induce the photodegradation of phenol, causing only less than 10% phenol degradation during 2 hours of irradiation. Pure TiO_2 (TiO_2) was able to completely abate phenol within 2 hours.

In the presence of COOH–GNP–TiO_2 and NH_2–GNP–TiO_2, the degradation was initially very slow (only 15% of phenol was abated during the first 30 min), then sped up (after 90 min, 50% or 60% of phenol disappears in the presence of COOH–GNP–TiO_2 or NH_2–GNP–TiO_2, respectively), and then, again, slowed down (after 2 h of irradiation, 40% and 30% of phenol was still present, in the presence of COOH–GNP–TiO_2 or NH_2–GNP–TiO_2, respectively). This behavior could be attributed to a modification of the materials or of the photogenerated reactant species occurring during irradiation. In fact, both COOH–GNP–TiO_2 and NH_2–GNP–TiO_2 changed color within a few minutes after the beginning of irradiation, and the grey suspensions turned to pale grey (Fig. S3†); however, after 30 min of irradiation the materials seemed to stabilize and did not further change color. Details about the transformation occurring on the material upon irradiation could be understood by measuring XPS spectra before and after 15 min of irradiation (Fig. S5†). The spectra collected after irradiation revealed the disappearance of the C 1s peak at 283.1 eV, associated to the GNP in close proximity to coordinatively unsaturated Ti atoms[31] and an increase in relative intensity of the

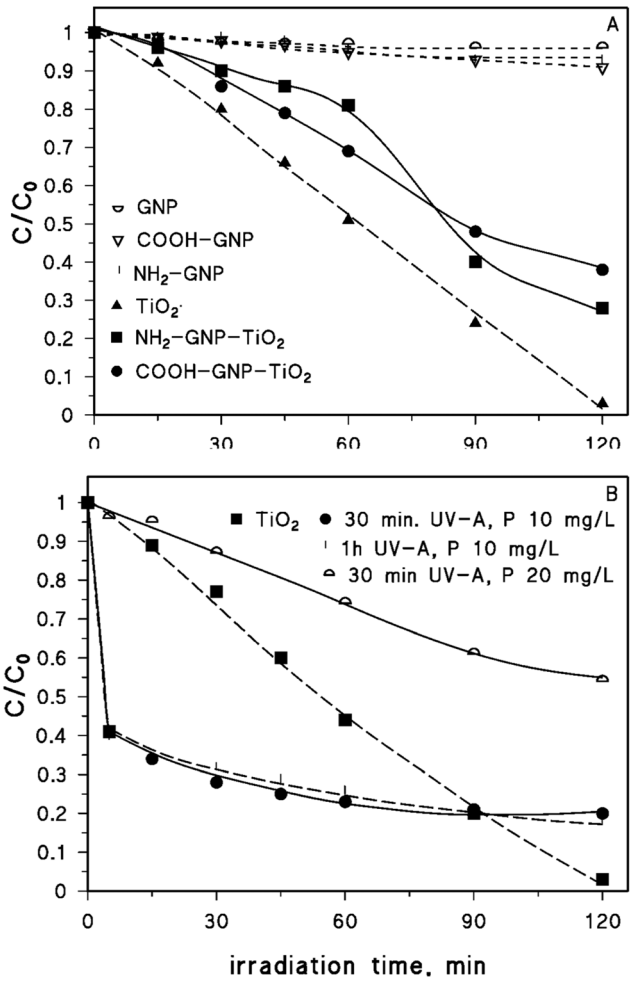

Fig. 1 Phenol (*P*) disappearance as a function of irradiation time. The conditions in all experiments are as follows: (A) *P* 10 mg L^{-1}; GNP (25 mg L^{-1}), COOH–GNP (25 mg L^{-1}), NH_2–GNP (25 mg L^{-1}), TiO_2 (1 g L^{-1}), NH_2–GNP–TiO_2 (1 g L^{-1}), COOH–GNP–TiO_2 (1 g L^{-1}); (B) pristine TiO_2 (1 g L^{-1}) and *P* added after 30 min or 1 h of COOH–GNP–TiO_2 (1 g L^{-1}) UV-A pre-irradiation (without *P*).

peaks at 286 eV and 288 eV, assigned to C–O and COOH groups, respectively.[31] These spectral changes suggest that after irradiation, GNP detached from the TiO_2 particles and became more oxidized.

To further understand the importance of this material transformation upon irradiation, we irradiated both COOH–GNP–TiO_2 and NH_2–GNP–TiO_2 for 30 min or 1 h without phenol and then repeated the experiments with phenol. The results are plotted in Fig. 1B, where COOH–GNP–TiO_2 UV-A activated materials are compared with pristine TiO_2. The two curves obtained after 30 min or 1 h of pre-irradiation following the addition of phenol at 10 mg L^{-1} are very similar, thus confirming the stabilization of the material suggested above. Phenol was degraded faster on the activated COOH–GNP–TiO_2 than on TiO_2 at the beginning of the experiment: almost 60% of phenol (C_0 = 10 mg L^{-1}) was degraded within 5 min of irradiation, and 80% phenol degradation was achieved within 30 min. A similar initial faster degradation followed by a slower reaction was found on the activated NH_2–GNP–TiO_2 (see Fig. S4†), although the overall degradation on this sample was much lower than on COOH–GNP–TiO_2. Thus, while before activation we could not observe a strong difference in photocatalytic efficiency between NH_2–GNP–TiO_2 and COOH–GNP–TiO_2, after UV-A activation COOH–GNP–TiO_2 became much more efficient than NH_2–GNP–TiO_2. This agrees with what we were expecting, since more oxidizing TiO_2 facets are exposed toward the solution in the COOH–GNP–TiO_2 sample.

We hypothesize that the reason for the instability of NH_2–GNP–TiO_2 and COOH–GNP–TiO_2 under irradiation and the different phenol degradation rates observed for these materials (Fig. 1A) is that some of the photogenerated species reacted with the hybrid materials. Photodegradation of reduced graphene oxide was indeed previously observed by Kamat and coworkers, especially for prolonged irradiation experiments, whereas for brief irradiations and in the presence of probes that can be easily oxidized and abated, such as methylene blue or rhodamine B, photocatalytic degradation of graphene is seldom observed.[35] In our case, the long irradiation experiments, necessary for phenol abatement, led to a change in the materials (Fig. S3 and XPS spectra in S5†) and a decrease in their photocatalytic activity. By pre-irradiating the samples (Fig. 1B), we completed the material transformation before phenol addition, thus allowing the phenol to be degraded in the absence of any competitive reaction.

The activated COOH–GNP–TiO_2 sample was much more effective at degrading phenol than the control TiO_2–TEOA sample at early degradation times (Fig. 1B). However, the kinetics slowed down at longer irradiation time, showing a trend that is consistent with second-order kinetics, where a reactant is limiting. To understand this phenomenon, we measured phenol degradation on these samples at different initial phenol concentrations (20 mg L^{-1}, plotted in Fig. 1B).

When the phenol concentration increased, the percentage of its abatement decreased and went from 80% to 46% on COOH–GNP–TiO_2. The concentration of phenol (P) as a function of irradiation time for a second order kinetics is expressed as:

$$\frac{P_t}{P_0} = \frac{P_0 - B_0}{P_0 - B_0(e^{-k(P_0 - B_0)t})} \quad (1)$$

where P_0 is the initial phenol concentration and B_0 is the concentration of the limiting reactant. By introducing $R = (A_0 - B_0)/A_0$, eqn (1) can be expressed as:

$$\frac{P_t}{P_0} = \frac{R}{1 - (1 - R)e^{-kRP_0t}} \quad (2)$$

From the data plotted in Fig. 1B, B_0 can be calculated as 8.6 ± 0.5 mg L^{-1}. Considering that oxygen content in GNP–COOH is very low (2.2%) and GNP content is below 5% (corresponding to a concentration lower than 50 mg L^{-1}) as estimated in the hybrid samples,[31] the limiting defective (and very reactive) species reactant can be ascribed to GNP itself rather than the functional groups on GNP.

3.2 Photo-induced phenol degradation with functionalized GNP/TiO_2 hybrids synthesized in the presence of shape controllers

To better control the morphology of the TiO_2 NPs in the GNP–TiO_2 hybrids and attempt to stabilize them, we introduced shape controllers in solution during the hydrothermal synthesis. We selected either EDA or OA because they are known to favor the growth of different crystalline facets ({100} and {101} for EDA and {001} for OA).[32] These facets will be oriented towards the solution, thus affecting the charge carrier separation process and therefore the photoactivity and the stability of the hybrid materials.[31]

3.2.1. Material characterization. Fig. 2 and S6† show the Raman spectra of COOH–GNP–TiO_2 and NH_2–GNP–TiO_2 prepared with EDA (COOH–GNP–TiO_2–EDA) or OA (COOH–GNP–TiO_2–OA) as shape controllers. The spectra are quite similar to

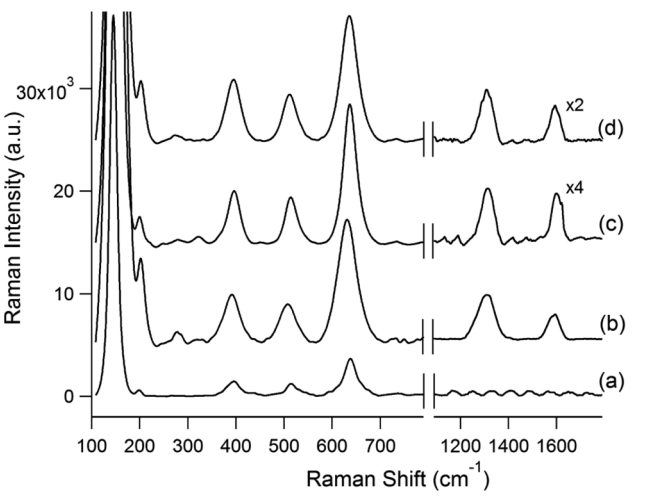

Fig. 2 Raman spectra of NH_2–GNP–TiO_2–EDA (a), NH_2–GNP–TiO_2–OA (b), COOH–GNP–TiO_2–EDA (c), and COOH–GNP–TiO_2–OA (d).

those observed for the samples prepared in the absence of shape controllers,[31] and they show that anatase was the only crystalline TiO_2 phase formed during the hydrothermal syntheses. Five well-resolved peaks can be identified in the range 150–650 cm^{-1}, localized at 144 cm^{-1} (E_g), 197 cm^{-1} (E_g), 395 cm^{-1} (B_{1g}), 513 cm^{-1} (B_{1g} + A_{1g}) and 634 cm^{-1} (E_g),[36] consistent with the characteristic vibrations for anatase. Additionally, two peaks at 1594 cm^{-1} and 1320 cm^{-1} are observed, which can be attributed to the GNP substrate: the peak at 1594 cm^{-1} corresponds to the Raman-active mode with symmetry E_{2g} and is characteristic of the presence of sp^2 C in graphene (G band), while the peak at 1320 cm^{-1} is associated with the presence of defects in the hexagonal C lattice (D band). The intensity ratio between TiO_2-related bands and G and D bands gives a qualitative measurement of the degree of association between TiO_2 and GNP, which decreases in the order NH_2–GNP–TiO_2–OA > COOH–GNP–TiO_2–OA > COOH–GNP–TiO_2–EDA > NH_2–GNP–TiO_2–EDA, for which close association between TiO_2 and GNP can be excluded.

Fig. 3–6 show the TEM images of all the samples prepared in the presence of shape controllers. The sample COOH–GNP–TiO_2–EDA shows both small (40–60 nm) and large (>100 nm) particles (Fig. 3). The smaller particles appear as rounded squares. These are likely to be truncated bipyramids with their *c* axis pointing outside the plane of the image,[37] which makes it hard to understand the extension of their crystalline facets. The bigger particles are quite elongated; since Raman shows that these are anatase, we can deduce that the {100} facets are more developed on these particles than the {101} facets. None of the TEM images showed TiO_2 NPs associated with GNP, thus suggesting that EDA favors homogeneous rather than heterogeneous nucleation.

On COOH–GNP–TiO_2–OA, most images show that the TiO_2 NPs are supported on GNP, which implies that the NPs nucleated and grew directly on graphene (Fig. 4). The particles are less elongated than those observed on COOH–GNP–TiO_2 (Fig. S1A† and ref. 31), *i.e.*, with a larger truncation ratio, and their projection on the micrograph is often a square. This implies that the presence of OA favors the growth of {100} and {001} facets at the expense of the {101},[32] giving the particles a pseudo-cubic appearance. The layer spacing is 0.36 nm (Fig. 4D; this is the characteristic spacing for anatase (101) planes, which can be detected on both {101} and {001} facets. This implies that the crystalline facet shown in Fig. 4d can be either the {101} facet of a bipyramid lying on the opposite {101} facet, or the top {001} facet of a particle with its *c* axis directed towards the observer (see Scheme S1†).

Similar considerations hold for the amino-functionalized samples: when EDA is added as shape controller (NH_2–GNP–TiO_2–EDA), elongated particles are obtained (Fig. 5). The spacing detected in Fig. 5b is again characteristic of the anatase (101) planes and can be present on both {101} and {001} facets, as discussed above. No evidence of GNP binding was observed, so that we can conclude that a homogeneous nucleation occurred.

Similarly to that observed on COOH–GNP–TiO_2–OA, the TiO_2 NPs nucleate and grow directly on GNP on the NH_2–GNP–TiO_2–OA sample. However, the NPs are less square, and their truncated bipyramidal shape is more evident. High-resolution images show again a plane spacing of 0.34 nm. However, since in this case the facets are trapezoidal, this spacing must refer to (101) planes found on {101} facets, thus suggesting a greater development of these facets on this sample.

A summary of the effect of the shape controllers on particle morphology is shown in Scheme 1. One of the main differences between the samples formed in the presence of OA and EDA is that those synthesized with EDA do not show TiO_2 NPs associated with GNP. This is consistent with the Raman results evidencing little (Fig. 2c) or no (Fig. 2a) presence of graphene peaks associated to TiO_2 NPs in the case of COOH–GNP–TiO_2–EDA and NH_2–GNP–TiO_2–EDA, respectively. We can explain this considering that EDA can easily be adsorbed on TiO_2 surface by forming EDA/TiO_2 complexes.[38] To prove this, we added EDA dropwise to a TiO_2 suspension; the well-dispersed suspension turned to deeply aggregated particles that settled down, as displayed in Fig. S7,† thus leading to more hydrophobic TiO_2 NPs. We hypothesize that this phenomenon isolates GNP from TiO_2 NPs, and that this in turn may prevent

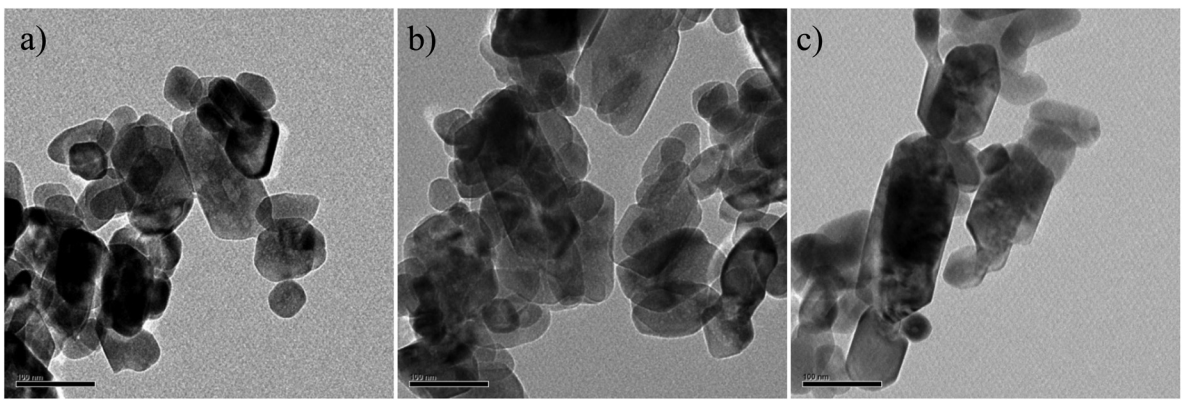

Fig. 3 TEM micrographs of COOH–GNP–TiO_2–EDA; scale bar is 100 nm in all panels.

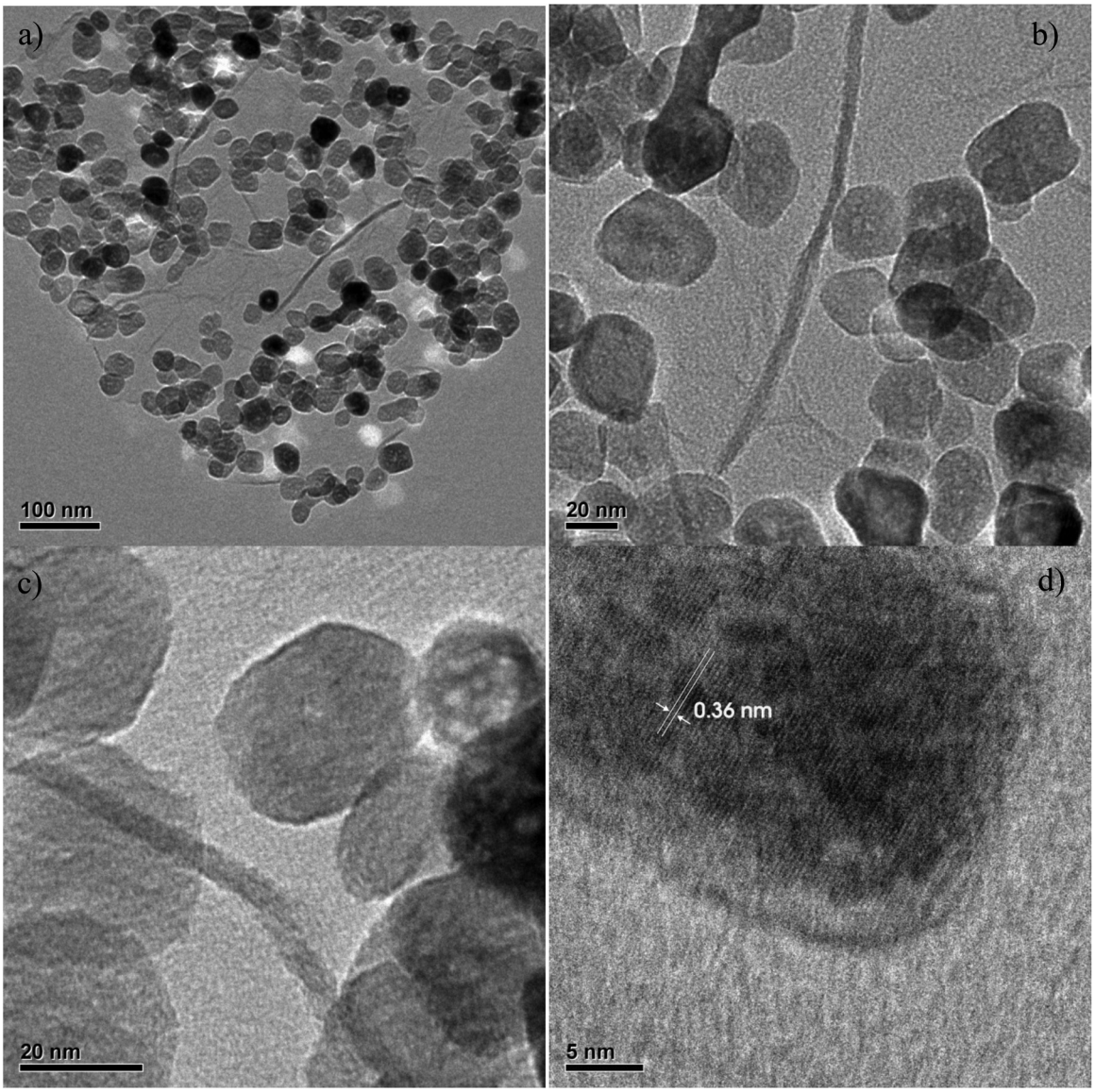

Fig. 4 Low (a) and high (b, c, d) magnification TEM micrographs of COOH–GNP–TiO_2–OA.

GNP degradation upon irradiation, while still maintaining the advantages of fast phenol degradation kinetics shown by the previous composites.

To prove this point, we proceeded with phenol degradation tests in the presence of COOH–GNP–TiO_2–EDA, NH_2–GNP–TiO_2–EDA, COOH–GNP–TiO_2–OA, and NH_2–GNP–TiO_2–OA.

3.2.2 Photocatalytic tests. The results of the photocatalytic degradation of phenol on the hybrid materials prepared with EDA and OA are shown in Fig. 7. Differently from NH_2–GNP–TiO_2 and COOH–GNP–TiO_2, all materials were stable under irradiation; no changes in color and in UV-Vis spectra were observed, even after long irradiation times.

The addition of shape controllers to COOH–GNP–TiO_2 (Fig. 7A) led to different results: while EDA improved the photocatalytic efficiency, OA had a detrimental effect. Within 120 min of irradiation, only 65% of phenol was abated on TiO_2–OA and even less (40%) on the composite material COOH–GNP–TiO_2–OA. Complete phenol degradation was achieved within 90 min of irradiation on COOH–GNP–TiO_2–EDA, while this took 120 min on pristine TiO_2. The low activity observed for COOH–GNP–TiO_2–OA may be attributed to the adsorption of OA on TiO_2 surfaces, leading to its inactivation. In fact, aliphatic carboxylic acids are known to adsorb on TiO_2 anatase and are employed in dye-sensitized solar cells to avoid direct contact between TiO_2 and electrolyte, thereby enhancing cell stability.[39]

The addition of shape controllers to NH_2–GNP–TiO_2 (Fig. 7B), instead, did not improve the photocatalytic efficiency of this sample; in particular, NH_2–GNP–TiO_2–OA showed the lowest activity. Since the sample NH_2–GNP–TiO_2–OA shows

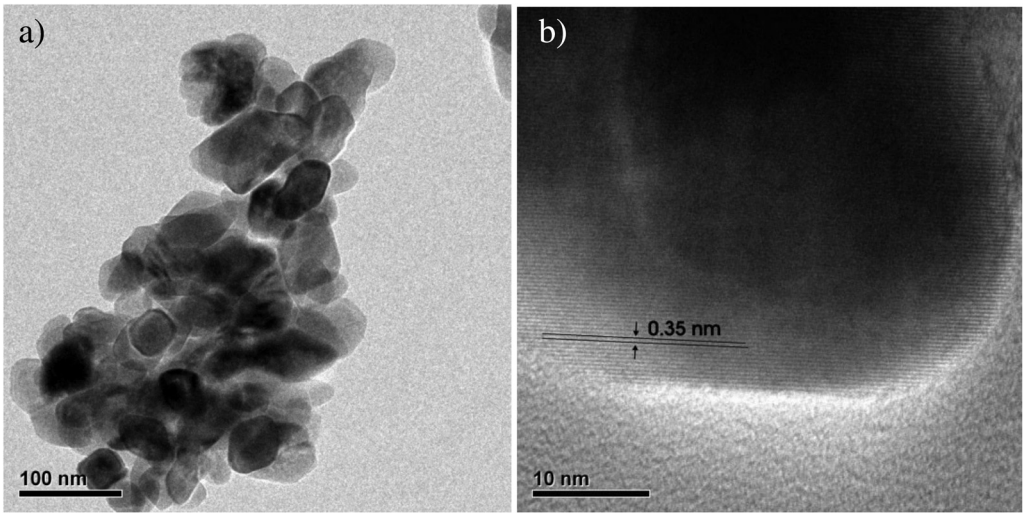

Fig. 5 Low (a) and high (b) magnification TEM micrographs of NH_2–GNP–TiO_2–EDA.

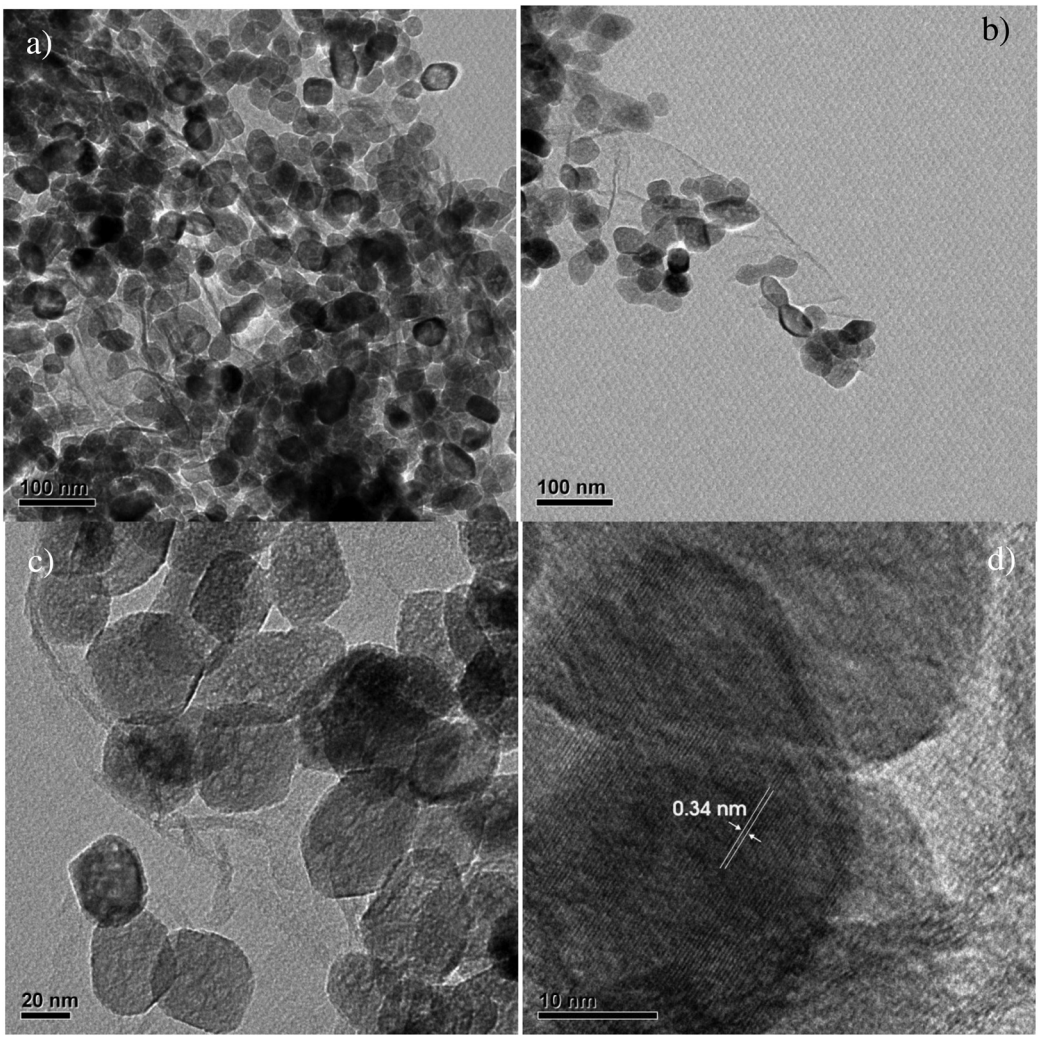

Fig. 6 Low (a, b) and high (c, d) magnification TEM micrographs of NH_2–GNP–TiO_2–OA.

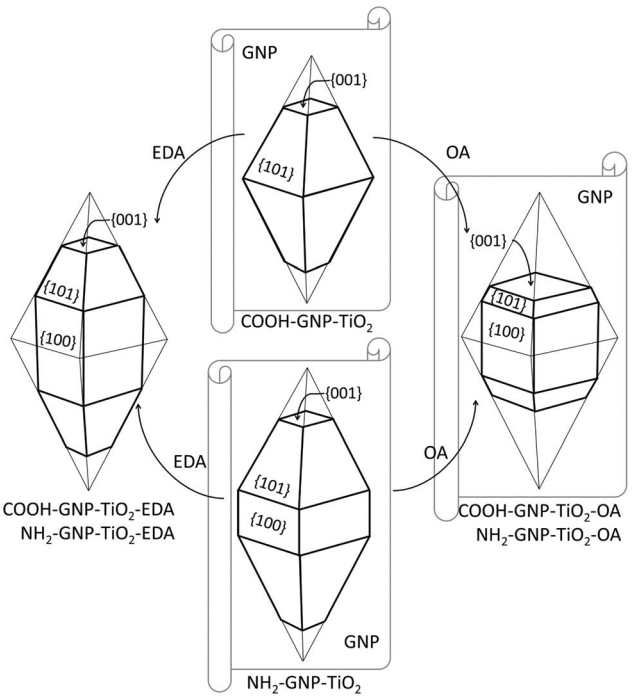

Scheme 1 Representation of the dominant particle morphology found in GNP–TiO_2 hybrid materials. While EDA leads to elongated, rod-like particles, OA favors pseudo-cubic shape. In the presence of EDA, homogeneous nucleation is favored over heterogeneous nucleation on GNP, which is instead observed in the presence of OA.

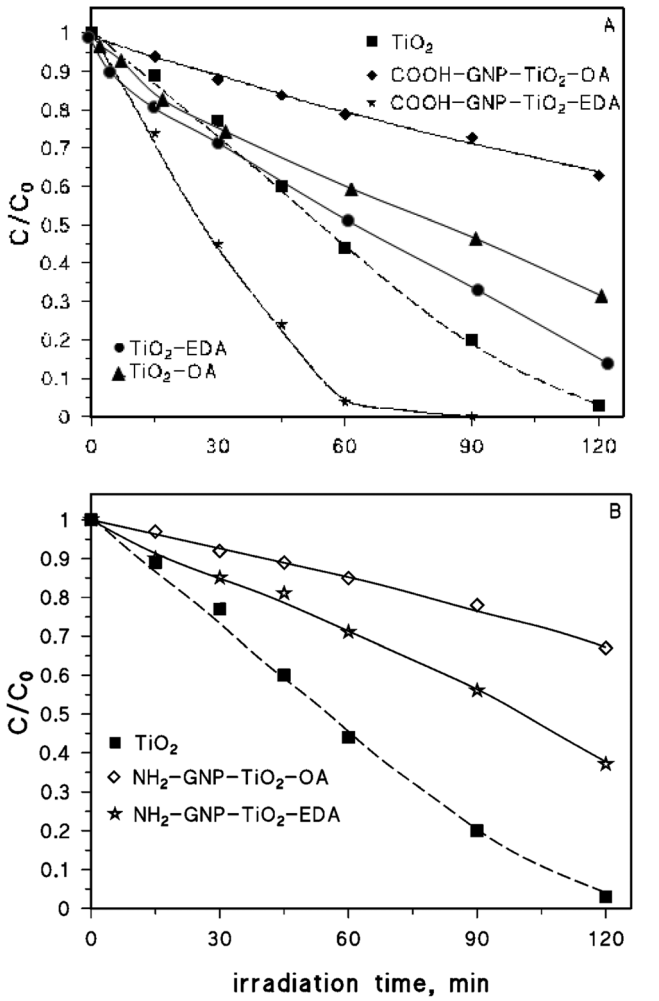

Fig. 7 Phenol (C_0 = 10 mg L^{-1}) disappearance as a function of irradiation time on materials prepared with shape controllers. (A) TiO_2 (1 g L^{-1}), TiO_2–EDA (1 g L^{-1}), TiO_2–OA (1 g L^{-1}), COOH–GNP–TiO_2–OA (1 g L^{-1}), COOH–GNP–TiO_2–EDA (1 g L^{-1}); (B) TiO_2 (1 g L^{-1}), NH_2–GNP–TiO_2–EDA (1 g L^{-1}), NH_2–GNP–TiO_2–OA (1 g L^{-1}).

morphology similar to NH_2–GNP–TiO_2 without the addition of shape controller, we do not expect, on the basis of the morphological analysis, an improvement in efficiency and stability under irradiation.

The fast kinetics observed in the presence of COOH–GNP–TiO_2–EDA (pseudo-first order kinetics similar to that observed on TiO_2, with $t_{1/2}$ of 30 min for the hybrid catalyst and $t_{1/2}$ 55 min for TiO_2) must be related to the preferential growth of more oxidizing {100} facets obtained in the presence of EDA, the more effective and selective hole transfer to phenol induced by synthesis in the presence of COOH–GNP, and the material stabilization due to the separation of GNP from TiO_2 NPs (Fig. 3) because of the presence of EDA. However, this result questions the role of GNP in improving the photocatalytic activity of TiO_2: if GNPs are separated from TiO_2, do they participate at all in the photocatalytic experiment?

To answer this question, we synthesized TiO_2 in the presence of EDA but without GNP (sample TiO_2–EDA), and then tested this material for its photocatalytic activity. The results for this material are plotted in Fig. 7A for comparison. We see a rate of phenol abatement very similar for TiO_2 and TiO_2–EDA, in both cases much lower than in the presence of COOH–GNP–TiO_2–EDA particles. This proves that GNP plays a crucial role in increasing phenol degradation rate when COOH–GNP–TiO_2–EDA particles are used, while EDA is responsible mostly for providing a loose coupling with GNP, thus reducing its degradation. The strong differences observed between COOH–GNP–TiO_2–EDA and COOH–GNP–TiO_2–OA seem to indicate that while OA non-specifically adsorbs on all TiO_2 facets, EDA specifically complexes the less active {101} facets, while the most active (and oxidative) {001} facets remain free.[32]

To rule out the possibility that the differences in photocatalytic activity that we measured were the results of different specific surface areas (SSA) of the samples, we estimated the SSA for the hybrid materials starting from TEM evidence (Table S1 in ESI†). The estimated SSA values ranged from 36 to 66 m^2 g^{-1}, and the lowest values were obtained for the samples with the largest particle size and the least close association with GNP, *i.e.* COOH–GNP–TiO_2–EDA (36 m^2 g^{-1}) and GNP–TiO_2 (40 m^2 g^{-1}). Therefore, the high activity of COOH–GNP–TiO_2–EDA cannot be ascribed to its SSA, since it is characterized by the lowest estimated SSA.

4. Conclusions

We have shown phase and shape control of TiO_2 NPs grown on carboxylic and amino-functionalized GNP, in the presence of OA and EDA in solution as additional shape controllers and material stabilizers. Among all materials synthesized, the COOH–GNP–TiO_2 hybrid prepared by adding EDA as shape controller exhibits the best performance toward phenol abatement, with almost twice as fast kinetics of phenol degradation than TiO_2 alone. We ascribe this result to the better charge carrier separation and loose coupling between COOH–GNP and TiO_2 NPs stabilized by EDA. The proximity between COOH–GNP and the reducing {101} facets of TiO_2 led to a more efficient transfer of photoelectrons, which in turn reduced charge recombination and improved the photoreduction reaction yield, while the lack of contact between the GNPs and TiO_2 prevented GNP degradation during the process. This result paves the way for a new generation of hybrid photocatalysts, which achieve better results thanks to their carefully controlled architecture.

Acknowledgements

This research is supported by a Marie Curie International Research Staff Exchange Scheme Fellowship (PHOTOMAT, proposal n. 318899) within the 7th European Community Framework Programme, the Natural Sciences and Engineering Research Council of Canada (NSERC), Fonds de recherche du Québec – Nature et technologies (FRQNT), Center for Self-assembled Chemical Structures (CSACS), Canada Research Chairs (CRC), the Canada Foundation for Innovation (CFI), and McGill Engineering Doctoral Award (MEDA).

References

1 A. Fujishima, K. Hashimoto and T. Watanabe, *TiO_2 Photocatalysis, Fundamentals and Applications*, Bkc Inc., Tokyo, 1999.
2 I. K. Konstantinou and T. A. Albanis, *Appl. Catal., B*, 2003, **42**, 319–335.
3 T. L. Thompson and J. T. Yates, *Jpn. Chem. Rev.*, 2006, **106**, 4428–4453.
4 P. Calza, V. A. Sakkas, C. Medana, A. A. Islam, E. Raso, K. Panagiotou and T. Albanis, *Appl. Catal., B*, 2010, **99**, 314–320.
5 C. Minero, G. Mariella, V. Maurino and E. Pelizzetti, *Langmuir*, 2000, **16**, 2632–2641.
6 N. Serpone and E. Pelizzetti, *Photocatalysis fundamentals and applications*, Wiley Interscience, Amsterdam, 1989.
7 X. Chen and S. S. Mao, *Chem. Rev.*, 2007, **107**, 2891–2959.
8 Y. Liu, L. Chen, J. Hu, J. Li and R. Richards, *J. Phys. Chem. C*, 2010, **114**, 1641–1645.
9 S. Livraghi, M. C. Paganini, E. Giamello, A. Selloni, C. D. Valentin and G. Pacchioni, *J. Am. Chem. Soc.*, 2006, **128**, 15666–15671.
10 H. Wang, T. You, W. Shi, J. Li and L. Guo, *J. Phys. Chem. C*, 2012, **116**, 6490–6494.
11 S. Hoang, S. P. Berglund, N. T. Hahan, A. J. Bard and C. B. Mullins, *J. Am. Chem. Soc.*, 2012, **134**, 3659–3662.
12 H. Kim, J. Kim and W. Choi, *J. Phys. Chem. C*, 2011, **115**, 9797–9805.
13 G. M. Veith, A. R. Lupini and N. J. Dudney, *J. Phys. Chem. C*, 2009, **113**, 269–280.
14 J. C. Yu, G. Li, X. Wang, X. Hu, C. W. Leung and Z. Zhang, *Chem. Commun.*, 2006, 2717–2719.
15 J. R. Raji and K. Palamivelu, *Ind. Eng. Chem. Res.*, 2011, **50**, 3130–3138.
16 W. Han, P. Liu, R. Yuan, J. Wang, Z. Li, J. Zhuang and X. Fu, *J. Mater. Chem.*, 2009, **19**, 6888–6895.
17 Y. J. Xu, Y. Zhuang and X. Fu, *J. Phys. Chem. C*, 2010, **114**, 2669–2676.
18 F. Zhang, X. Carrier, J. M. Krafft, Y. Yoshimura and J. Blanchard, *New J. Chem.*, 2010, **34**, 508.
19 Q. Xiang, J. Yu and M. Jaroniec, *J. Am. Chem. Soc.*, 2012, **134**, 6575–6578.
20 H. Zhang, X. Lu, Y. Li and J. Wang, *ACS Nano*, 2011, **5**, 590–596.
21 K. Li, J. Xiong, T. Chen, L. Yan, Y. Dai, D. Song, Y. Lu and Z. Zeng, *J. Hazard. Mater.*, 2013, **250**, 19–28.
22 K. Li, T. Chen, L. Yan, Y. Dai, Z. Huang, J. Xiong, D. Song, Y. Lu and Z. Zeng, *Colloids Surf., A*, 2013, **422**, 90.
23 O. Akhavan and E. Ghaderi, *J. Phys. Chem. C*, 2009, **113**, 20214–20220.
24 H. Wang, T. Maiyalagan and X. Wang, *ACS Catal.*, 2012, **2**, 781–794.
25 U. Diebold, *Surf. Sci. Rep.*, 2003, **48**, 53–229.
26 T. Taguchi, Y. Saito, K. Sarukawa, T. Ohno and M. Matsumura, *New J. Chem.*, 2003, **27**, 1304–1306.
27 C. Z. Wen, H. B. Jiang, S. Z. Qiao, H. G. Yang and G. Q. Lu, *J. Mater. Chem.*, 2011, **21**, 7052–7061.
28 T. Tachikawa, N. Wang, S. Yamashita, S.-C. Cui and T. Majima, *Angew. Chem., Int. Ed.*, 2010, **49**, 8593–8597.
29 T. Ohno, K. Sarukawa and M. Matsumura, *New J. Chem.*, 2002, **26**(9), 1167–1170.
30 P. V. Kamat, *J. Phys. Chem. Lett.*, 2011, **2**(3), 242–251.
31 F. Sordello, G. Zeb, K. Hu, P. Calza, C. Minero, T. Szkopek and M. Cerruti, *Nanoscale*, 2014, **6**, 6710–6719.
32 T. Sugimoto, X. Zhou and A. Muramatsu, *J. Colloid Interface Sci.*, 2003, **259**(1), 53–61.
33 K. J. Huang, D. J. Niu, X. Liu, Z. W. Wu, Y. F. Fan and Y. Y. Wu, *Electrochim. Acta*, 2010, **56**, 2947–2953.
34 P. Calza, L. Rigo and M. Sangermano, *Appl. Catal., B*, 2011, **106**, 657–665.
35 J. G. Radich, A. L. Krenselewski, J. Zhu and P. V. Kamat, *Chem. Mater.*, 2014, **26**(15), 4662–4668.
36 T. Ohsaka, F. Izumi and Y. Fujiki, *J. Raman Spectrosc.*, 1978, **7**, 321–324.
37 C. Deiana, M. Minella, G. Tabacchi, V. Maurino, E. Fois and G. Martra, *Phys. Chem. Chem. Phys.*, 2013, **15**(1), 307–315.
38 E. Farfan-Arribas and R. J. Madix, *J. Phys. Chem. B*, 2003, **107**, 3225–3233.
39 J. Lim, Y. S. Kwon and T. Park, *Chem. Commun.*, 2011, **47**, 4147–4149.